Structural, spectroscopic, and tunable laser properties of Yb³⁺-doped NaGd(WO₄)₂

C. Cascales, M. D. Serrano, F. Esteban-Betegón, and C. Zaldo

Instituto de Ciencia de Materiales de Madrid, Consejo Superior de Investigaciones Científicas, Calle Sor Juana Inés de la Cruz 3, Cantoblanco, E-28049 Madrid, Spain

R. Peters, K. Petermann, and G. Huber

Institut für Laser-Physik, Universität Hamburg, Luruper Chaussee 149, D-22761 Hamburg, Germany

L. Ackermann, D. Rytz, and C. Dupré

FEE, Struthstr. 2, D-55743 Idar-Oberstein, Germany

M. Rico, J. Liu, U. Griebner, and V. Petrov[*]

Max-Born-Institute for Nonlinear Optics and Ultrafast Spectroscopy, 2A Max-Born-Str., D-12489 Berlin, Germany

(Received 2 July 2006; published 20 November 2006)

Single crystals of Yb³⁺-doped NaGd(WO₄)₂ with up to 20 mol % ytterbium content have been grown by the Czochralski technique in air or in N_2+O_2 atmosphere and cooled to room temperature at different rates (4–250 °C/h). Only the noncentrosymmetric tetragonal space group $I\bar{4}$ accounts for all reflections observed in the single crystal x-ray diffraction analysis. The distortion of this symmetry with respect to the centrosymmetric tetragonal space group $I4_1/a$ is much lower for crystals cooled at a fast rate. Na⁺, Gd³⁺, and Yb³⁺ ions share the two nonequivalent $2b$ and $2d$ sites of the $I\bar{4}$ structure, but Yb³⁺ (and Gd³⁺) ions are found preferentially in the $2b$ site. Optical spectroscopy at low (5 K) temperature provides additional evidence of the existence of these two sites contributing to the line broadening. The comparison with the $^2F_{7/2}(n)$ and $^2F_{5/2}(n')$ Stark energy levels calculated using the crystallographic Yb-O bond distances allows to correlate the experimental optical bands with the $2b$ and $2d$ sites. As a novel uniaxial laser host for Yb³⁺, NaGd(WO₄)₂ is characterized also with respect to its transparency, band-edge, refractive indices, and main optical phonons. Continuous-wave Yb³⁺-laser operation is studied at room temperature both under Ti:sapphire and diode laser pumping. A maximum slope efficiency of 77% with respect to the absorbed power is achieved for the π polarization by Ti:sapphire laser pumping in a three-mirror cavity with Brewster geometry. The emission is tunable in the 1014–1079 nm spectral range with an intracavity Lyot filter. Passive mode locking of this laser produces 120 fs long pulses at 1037.5 nm with an average power of 360 mW at ≈97 MHz repetition rate. Using uncoated samples of Yb:NaGd(WO₄)₂ at normal incidence in simple two-mirror cavities, output powers as high as 1.45 W and slope efficiencies as high as 51% are achieved with different diode laser pump sources.

I. INTRODUCTION

Double tungstate (DT) and double molybdate (DM) compounds with the general formula $MT(XO_4)_2$, where M is a monovalent alkali cation (Li-Cs), T is a trivalent cation (Al, Ga, In, Cr, Bi, Y, La, or lanthanide Ln=Ce-Lu), and $X=$W or Mo, may exhibit ordered phases with separate sites for M and T cations and disordered phases where M and T cations are randomly distributed over the same cationic sublattice.[1] Their structure is related to the Ca²⁺ ion substitution in the CaXO_4 tetragonal scheelite-type structure by a pair of M^+ and T^{3+} cations. Some of the ordered phases like the strongly anisotropic (biaxial) monoclinic KGd(WO₄)₂ and KY(WO₄)₂ are established Ln³⁺ ion laser hosts with very large absorption and emission cross sections of the active dopant, e.g., Nd³⁺, Yb³⁺, Ho³⁺, or Tm³⁺. The disordered tetragonal phases are interesting because of their extended potential for tunable laser operation and generation of ultrashort optical pulses, and also because their uniaxial character leads to less anisotropy in the optomechanical properties which is important for the processing of active elements and their thermal management. The random distribution of M^+ and T^{3+} cations in tetragonal DTs and DMs induces a locally variable crystal field acting on the dopant ion which is expressed in the large bandwidths of the spectral lines of the electronic transitions for the rare-earth elements. Concerning their optomechanical and spectroscopic properties, such disordered crystals occupy an intermediate position between ordered laser hosts and glasses. Some of them (e.g., $M=$Na and $T=$La, Nd··Er or Bi) melt congruently and can be pulled in large sizes by the Czochralski (Cz) technique. Moreover, these same compounds do not experience destructive phase transformations upon cooling from their growth temperature and as a consequence defect free boules with tetragonal crystalline symmetry can be obtained at room temperature.

Although different Ln-dopant and host combinations were studied in the past, both for ordered and disordered DT and DM crystals, most of the laser related activities were focused on the Nd³⁺ ion. More recently the interest has shifted towards the Yb³⁺ ion which provides better possibilities for power scaling in the same 1 μm spectral range and possesses several other attractive properties: i) Due to the strong electron-phonon coupling of Yb³⁺ to the lattice, this ion ex-

hibits linewidths which are intrinsically broader than those for the Nd^{3+} ion, ii) The Yb^{3+} ion exhibits longer energy-storage lifetime and smaller quantum defect (less heat generation) than Nd^{3+}, iii) It can be pumped by the optically more robust InGaAs diode lasers operating in the 900–1000 nm spectral range, and iv) The relatively simple two-manifold structure of Yb^{3+} prohibits undesired excited-state absorption, up-conversion and cross-relaxation processes.

$NaGd(WO_4)_2$ (NaGdW) doped with Nd^{3+} and grown by the Cz method, was the first disordered crystal of this type for which lasing at 77 K with flash-lamp pumping was demonstrated as early as 1964.[2] The same host-dopant combination was also the first one of that kind for which diode-pumped room temperature continuous-wave (CW) operation was reported more than 30 years later.[3] In 2004 we achieved for the first time lasing of the Yb^{3+} ion in such type of disordered crystal, using again NaGdW as host.[4,5] Soon after that, Yb^{3+} laser operation was reported in several related DT and DM hosts, namely $NaLa(WO_4)_2$,[6,7] $NaLa(MoO_4)_2$,[6,8,9] and $LiGd(MoO_4)_2$,[10] see Ref. 11 for a review. Very recently some thermomechanical properties of NaGdW like the thermal expansion and conductivity coefficients were studied.[12,13] The aim of the present work is to evaluate the potential for laser operation of Yb^{3+}-doped $NaGd(WO_4)_2$ or shortly Yb:NaGdW with special emphasis on the tunability which is related to the spectral linewidths. For this purpose the growth and the structural, optical, and spectroscopic properties of this crystal are studied for several Yb doping levels. Substantial improvement of the CW laser performance in terms of efficiency and output power, both with Ti:sapphire and diode laser pumping, is achieved in comparison to the initial results.[4,5] Tunable and mode-locked femtosecond laser operation is also demonstrated.

II. CRYSTAL GROWTH AND STRUCTURE OF UNDOPED AND YTTERBIUM DOPED SODIUM GADOLINIUM TUNGSTATE

Undoped and Yb^{3+}-doped NaGdW single crystals were grown by the Cz technique using a diameter control system and Gd_2O_3, Yb_2O_3, Na_2CO_3 and WO_3 as starting materials. The molar ratio of Yb_2O_3 and $Yb_2O_3+Gd_2O_3$ in the melt will be denoted as x. Three sets of experimental growth conditions were used:

i) Cz1: Yb:NaGdW crystals with $x=0$, 0.05, 0.1, 0.2 were pulled in air from the stoichiometric melt. More details about this synthesis procedure can be found elsewhere.[4] The raw materials used (Alfa Aesar) had a purity of 99.99% except for WO_3 for which the purity was 99.8%. For homogenization, the melt in the 75 cc Pt crucible was heated to 25 °C above the melting point and kept for one hour at this temperature. The optimum crystallization temperature was determined by monitoring the crucible weight when seeding with a **c**-cut NaGdW crystal rod. The rotation and pulling rates were 10 rpm and 2–2.3 mm/h, respectively. The grown crystals were cooled to room temperature at a standard rate of 10 °C/h. The crystals obtained were colorless. The typical dimensions of the pulled boules were 20 mm (diameter)

and 50 mm (length). Two further Yb^{3+}-doped crystals with $x=0.01$ were grown from 5 wt % $Na_2W_2O_7$ enriched melt (this decreases the melting temperature of the mixture). These two crystals were cooled at 250 °C/h and 4 °C/h, respectively. The actual Yb content in the grown crystals was determined for the samples with $x=0.1$ and 0.2 by inductively coupled plasma atomic emission spectrometry (ICP-AES) and microprobe analysis, respectively. The obtained Yb concentrations were 5.1×10^{20} cm^{-3} and 10.9×10^{20} cm^{-3}, respectively. Thus the Yb segregation coefficient was in the 0.8–0.85 range.

ii) Cz2: Yb:NaGdW crystals with $x=0.01 \cdots 0.3$ were pulled also in air from the stoichiometric melt using 6.5–8 cc Pt crucibles. This allowed the use of raw materials with much higher purity, 99.999%, except for Na_2CO_3 with 99.995%. The mixture was heated to 30 °C above the melting point and kept for one hour at this temperature for homogenization. The rotation and pulling rates were 19 rpm and 3 mm/h, respectively. A Pt wire was used as a seed and the grown crystals were cooled to room temperature at a rate of 80 °C/h. The boules with a diameter of $\approx$10 mm and a length between 10 and 15 mm had a weight of the order of 10 g. No cracking occurred up to a doping level of $x=0.1$ but for higher Yb concentrations the pulling rate had to be reduced to 1 mm/h in order to avoid this. The actual Yb content in the grown crystals was measured by microprobe analysis. The obtained segregation coefficient varied from 0.67 to 0.87.

iii) Cz3: Yb:NaGdW crystals with $x=0 \cdots 0.13$ were pulled in nitrogen plus small quantity of air with 5 mol % $Na_2W_2O_7$ flux added to the melt. The crystal rotation and pulling rates were 12 rpm and 0.5–0.7 mm/h, respectively. The seed was a cylinder of NaGdW with a diameter of 7 mm, and a length of 20 mm oriented along the **c** axis. A 400 cc Ir crucible and chemicals of purity better than 99.99% were used in this case. The cooling rate to room temperature was about 40 °C/h. The cylindrical boules obtained had a weight of about 200 g, a diameter of 25 mm, and a length between 60 and 80 mm. The segregation coefficient of Yb^{3+} determined as in Cz2 ranged between 0.61 and 0.79.

The crystalline structure of NaGdW has been the subject of several previous studies. In an early work devoted to it, only a tetragonal structure was specified.[14] Subsequently, from powder x-ray diffraction (XRD) data, NaGdW was identified to be isostructural to $CaWO_4$, scheelite,[15,16] with the centrosymmetric space group (SG) $C_{4h}^6 \equiv I4_1/a$ (No. 88). In a more recent work the refinement was also carried out in the scheelite SG but these authors observed splitting of the 101, 112, and 211 Bragg reflections in oxygen deficient crystals with a green color.[17] Partial lattice ordering due to the different ionic radii of Na^+ and Gd^{3+} accompanied by symmetry reduction and/or superlattice formation were suggested as possible mechanisms for this effect. The presence of the smaller Yb^{3+} ions should favor this process of ordering in Yb:NaGdW.[17,18] Despite this existing assignment, the tetragonal noncentrosymmetric space group $S_4^2 \equiv I\bar{4}$ (No. 82) is an alternative already considered for some disordered DTs and DMs of the same type, e.g., $LiGd(MoO_4)_2$ and $NaBi(WO_4)_2$.[10,19] The accurate determination of the symme-

TABLE I. Assessment of the $I4_1/a \rightarrow I\bar{4}$ distortion of Yb:NaGdW from the individual scan intensity measurements.

Yb:NaGdW, x (melt) Growth conditions		0 Cz1	0.01 Cz2	0.05 Cz3	0.2 Cz1	0.25 Cz2	0.3 Cz2
$00l$, l even and $\neq 4n$:	002	42	38	18	89	175	20
	006	3	4	2	23	16	13
	0010	3	3	4	7	6	3
$h\bar{h}0$, $h \neq 2n$:	$1\bar{1}0$	18	30	20	46	39	41
	$3\bar{3}0$	4	5	3	3	7	5
EB[a]		3	5	4	6	5	4

[a]In order to define a proper intensity reference, the estimated background (EB) is calculated as the average value of several measured reflections $00l$ with $l \neq 2n$ which are forbidden in the three tetragonal space groups considered.

try of NaGdW and Yb:NaGdW crystals is essential for the correct interpretation of the observed Yb^{3+} spectroscopic characteristics: In the $I4_1/a$ symmetry, a single lattice site $4b$ is 50% filled with Na^+ and 50% with the trivalent cations (Gd^{3+} and/or Yb^{3+}) in a random distribution for the first cationic sphere of neighbors, while for the $I\bar{4}$ symmetry two different crystallographic sites $2b$ and $2d$ exist, and each of them can accommodate both the monovalent and the trivalent cations but in general with different occupancy factors (OFs). The multiple local environments associated with the random cationic occupancy of the host sites give rise to a crystal-field distribution around Yb^{3+} which may result in some spectral structure of its optical bands that can be resolved at low temperature as already demonstrated for Nd^{3+} in $NaBi(WO_4)_2$.[20] The observed total bandwidth is determined by a convolution of the lineshapes due to the local environments over the different sites, therefore *a priory* it can be expected that it will be larger for an increasing number of Yb^{3+} sites.

The procedure used in the present work for determination of the correct structure consisted in an initial evaluation at room temperature of the significance of some hkl reflections which are systematically absent in the SG $I4_1/a$, through their individual psi-scan intensity measurements. This has been performed on an Enraf-Nonius CAD4 diffractometer with Mo $K\alpha$ radiation, for undoped and some representative Yb^{3+}-doped NaGdW crystals. The reflections selected for this purpose were those constituting violations of the a plane, $h\bar{h}0$, where $h \neq 2n$, which are allowed not only for SG $I\bar{4}$ but also for SG $C_4^6 \equiv I4_1$ (No. 80), as well as those forbidden for the 4_1 axis, $00l$, where l is even but $l \neq 4n$, which are allowed only for SG $I\bar{4}$. The average values obtained from several collections of each of the above reflections were then compared, for the separate crystals, with the estimated background (EB) intensity obtained from averaging of $00l$ reflections, $l \neq 2n$, which are forbidden in all these SGs. It can be seen from Table I that the intensity of the selected reflections, in particular that of 002 and $1\bar{1}0$, is well above the EB level for all crystals studied which leads to the conclusion that only the SG $I\bar{4}$ can adequately describe the experimental XRD data.

In a second step, we performed single crystal XRD analysis of undoped and Yb^{3+}-doped NaGdW crystals grown under the conditions described before. These data were collected at room temperature using a Siemens SMART CCD diffractometer equipped with a normal focus 3 kW sealed tube. Small prismatic single crystals were cut for this purpose in order to avoid the possibility of selecting a twinned crystal and to minimize the absorption effect. The data was collected over a quadrant of the reciprocal space by a combination of three sets of exposures. Each set had a different φ angle for the crystal and each exposure of 20 s covered 0.3° in ω. The crystal-to-detector separation was 5.08 cm. Further details are provided in Table II. Neutral atom scattering factors for all atoms were used, and anomalous dispersion corrections were applied. All calculations were performed using the SHELXTL program.[21]

The refinement of the crystal structure, i.e., the determination of the unit cell parameters, the atomic coordinates, the OFs for Na and Gd/Yb in the shared cationic positions, $2d(\text{I})$ and $2b(\text{II})$, in combination with the low R_1 discrepancy factors and the positive thermal anisotropic displacements for most of the atoms, allowed to conclude about the presence of a certain number of systematic absence exceptions for the a plane and the 4_1 axis, with intensity $I > 3\sigma(F)$ where F is the structure factor. These systematic absence exceptions are well above the $I > 2\sigma(I)$ threshold for the reflections considered in the refinement which is a clear indication for the noncentrosymmetric SG $I\bar{4}$. All these results are included in Table II and several important conclusions can be derived from them:

i) The symmetry of the undoped NaGdW host is $I\bar{4}$, with a certain degree of structural order over the $2d(\text{I})$ and $2b(\text{II})$ sites, i.e., the cationic distribution does not correspond to the statistical one over both S_4 centers.

ii) The incorporation of Yb^{3+} suggests modification of the crystal structure in two ways: a) The relative intensity of the $00l$ and $h\bar{h}0$ reflections increases, i.e., the distortion of the doped crystals from the centrosymmetric SG $I4_1/a$ towards the noncentrosymmetric SG $I\bar{4}$ increases, and b) the cationic order over the $2d$ and $2b$ sites also increases with the Yb content.

TABLE II. Crystal data at 296(2) K and structure refinement details for undoped and Yb-doped NaGdW crystals.

Nominal formula in melt Growth conditions				NaGd(WO$_4$)$_2$[a–c] Cz1				Yb:NaGd(WO$_4$)$_2$ ($x=0.05$)[a–c] Cz3				Yb:NaGd(WO$_4$)$_2$ ($x=0.2$)[a–c] Cz1				Yb:NaGd(WO$_4$)$_2$ ($x=0.25$)[a–c] Cz2			
Unit cell dimensions (Å)				$a=b=5.2440(5)$ $c=11.3794(14)$				$a=b=5.2450(5)$ $c=11.3875(16)$				$a=b=5.2406(6)$ $c=11.3670(18)$				$a=b=5.2321(7)$ $c=11.352(2)$			
Volume (Å^3)				312.93(6)				313.27(6)				312.16(7)				310.76(8)			
Z, Calculated density (Mg/m^3)				2, 7.230				2, 7.283				2, 7.322				2, 7.321			
Absorption coefficient (mm^{-1})				47.216				47.164				47.332				47.545			
Crystal size (mm^3)				$0.10\times0.09\times0.05$				$0.12\times0.06\times0.05$				$0.12\times0.07\times0.04$				$0.12\times0.08\times0.05$			
θ range for data collection (°)				3.58 to 29.07				3.58 to 28.89				3.58 to 28.53				3.59 to 26.35			
hkl Limiting indices				−2 to 7, −6 to 6, −11 to 7				−6 to 3, −4 to 7, −15 to 11				−6 to 3, −6 to 6, −10 to 8				−6 to 1, −6 to 6, −13 to 13			
Reflections collected/unique				784/305 [R(int)$=0.0409$]				798/358 [R(int)$=0.0393$]				758/284 [R(int)$=0.0382$]				593/266 [R(int)$=0.0373$]			
Data/restraints/parameters				305/2/32				358/2/34				284/2/34				266/2/34			
Goodness-of-fit on F^2				1.147				1.087				1.114				1.152			
Final R indices [$I>2\sigma(I)$]				$R_1=0.0661$, $wR_2=0.1707$				$R_1=0.0396$, $wR_2=0.1029$				$R_1=0.0610$, $wR_2=0.1452$				$R_1=0.0524$, $wR_2=0.1369$			
R indices (all data)				$R_1=0.0683$, $wR_2=0.1736$				$R_1=0.0458$, $wR_2=0.1069$				$R_1=0.0636$, $wR_2=0.1500$				$R_1=0.0536$, $wR_2=0.1389$			
Extinction coefficient				0.086(16)				0.086(14)				0.06(3)				0.093(19)			
Atom, site, x, y, z, U(eq)[d]	Na(I)/T(I)	2d	$\frac{1}{2}$	0	$\frac{1}{4}$	13(3)	$\frac{1}{2}$	0	$\frac{1}{4}$	6(3)	$\frac{1}{2}$	0	$\frac{1}{4}$	1(6)	$\frac{1}{2}$	0	$\frac{1}{4}$	7(3)
	Na(II)/T(II)	2b	$\frac{1}{2}$	$\frac{1}{2}$	0	18(3)	$\frac{1}{2}$	$\frac{1}{2}$	0	11(3)	$\frac{1}{2}$	$\frac{1}{2}$	0	12(5)	$\frac{1}{2}$	$\frac{1}{2}$	0	23(2)
	W(1)	2a	0	0	0	15(2)	0	0	0	11(1)	0	0	0	7(3)	0	0	0	14(1)
	W(2)	2c	0	$\frac{1}{2}$	$\frac{1}{4}$	15(2)	0	$\frac{1}{2}$	$\frac{1}{4}$	8(1)	0	$\frac{1}{2}$	$\frac{1}{4}$	9(3)	0	$\frac{1}{2}$	$\frac{1}{4}$	17(2)
	O(1)	8g[e]	2390(20)	1530(20)	842(16)	19(4)	2370(30)	1540(30)	879(15)	15(4)	2400(40)	1530(30)	850(30)	17(7)	2386(19)	1561(17)	857(13)	23(3)
	O(2)	8g[e]	2430(20)	3460(20)	1655(16)	20(4)	2500(30)	3490(40)	1652(18)	17(5)	2440(40)	3470(40)	1660(30)	19(7)	2430(50)	3484(17)	1687(12)	19(3)
OF[f]	Na(I)/T(I)	2d	0.55(2)/ 0.45(2)				0.56(2)/ 0.44(4)				0.58(5)/ 0.41(7)				0.59(2)/ 0.42(4)			
	Na(II)/T(II)	2b	0.41(2)/ 0.59(2)				0.38(2)/ 0.61(4)				0.35(3)/ 0.65(6)				0.39(2)/ 0.62(4)			
Systematic absence exceptions:																			
hkl $I>3\sigma(F)$ for 4_1 axis [total $I>2\sigma(I)$]				1 (2)				2 (7)				2 (2)				2 (2)			
hkl $I>3\sigma(F)$ for a plane [total $I>2\sigma(I)$]				4 (20)				4 (13)				4 (21)				5 (16)			
x-ray crystal refined composition				Na$_{0.96(2)}$Gd$_{1.04(2)}$(WO$_4$)$_2$				Na$_{0.94(2)}$Gd$_{1.02(4)}$Yb$_{0.04(4)}$(WO$_4$)$_2$				Na$_{0.93(5)}$Gd$_{0.89(6)}$Yb$_{0.17(7)}$(WO$_4$)$_2$				Na$_{0.97(2)}$Gd$_{0.82(4)}$Yb$_{0.22(4)}$(WO$_4$)$_2$			

[a]XRD wavelength 0.71073 (Å).
[b]XRD absorption correction SADABS.
[c]Refinement method: full matrix least squares on F^2.
[d]$U_{(eq)}$ is defined as one third of the trace of the orthogonalized U_{ij} tensor.
[e]Atomic coordinates $\times10^4$.
[f]Occupancy factor for the indicated site. They were refined with no restrains between 2b and 2d sites.
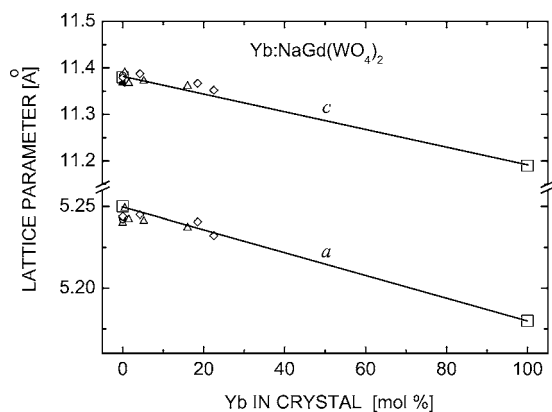
FIG. 1. Evolution of the Yb:NaGdW crystal unit cell parameters versus Yb content in the crystal: ◇ this work (single crystal XRD), □ Rode *et al.* (powder XRD) (Ref. 15), △ Zharikov *et al.* (powder XRD of ground crystal) (Ref. 17), ○ Mokhosoev *et al.* (powder XRD) (Ref. 14), ◀ JCPDS 25-0829 (powder XRD) (Ref. 16) The lines connect the values of Rode *et al.* (Ref. 15).

iii) All crystals studied clearly exhibit Na^+ deficiency which is typically of the order of 5 mol % but in some exceptional cases was as large as 14 mol % ($x=0.3$ sample grown under Cz2 conditions). This deficit is partially compensated by excess incorporation of trivalent ions (Gd^{3+} and Yb^{3+}) which reached in some exceptional cases ($x=0.23$, Cz2) 21 mol %. The electric charge compensation is achieved by W^{6+} vacancies, typically of the order of 1 mol % but in some exceptional cases ($x=0.23$, Cz2) reaching 5 mol %. This was confirmed by microprobe analysis. These results are consistent with the well known Na and W volatilities during the growth process. The compounds formed after resolidification of the vapors emitted by the melt were identified as a sodium tungsten bronze, i.e., a phase resulting from the intercalation of Na in WO_3, Na_xWO_3, $x<1$.[22]

iv) The unit cell parameters of Yb:NaGdW ($x=0\cdots0.25$) crystals decrease with the Yb^{3+} concentration as shown in Fig. 1, where data from the literature is included for comparison. Most of the results previously reported agree with the observed trend within the experimental uncertainties. The only exception concerns a report on $NaYb(WO_4)_2$,[23] but since the deviation in this work is substantial, it can be obviously discarded.

Furthermore, we studied the influence of the cooling rate of grown crystals on the resulting structure. For this purpose, the two samples of Yb:NaGdW grown with $x=0.01$ under the Cz1 conditions with very different cooling rates were considered as two limiting cases. Both samples were analyzed by single crystal XRD. The crystallographic data for the crystal cooled at 4 °C/h was very similar to that of undoped NaGdW cooled at 10 °C/h. For the crystal cooled at 250 °C/h, however, the collected *hkl* Bragg reflections not allowed by the SG $I4_1/a$ had intensities always lower than $3\sigma(F)$. The refinement (using the same set of *hkl* reflections) of the XRD data for this crystal in the $I4_1/a$ and $I\bar{4}$ symmetries resulted in lower R_1 for the centrosymmetric SG $I4_1/a$. These results clearly indicate that although upon rapid post-

growth cooling again only the SG $I\bar{4}$ can account for all observed reflections, the deviation from the centrosymmetric SG $I4_1/a$ is much lower than for crystals cooled at the "standard" rate (10 °C/h). Thus, it turns out that the combination of slow cooling rates and high Yb^{3+}-concentration leads to the largest distortion from the centrosymmetric SG.

III. OPTICAL AND RAMAN PROPERTIES OF UNDOPED AND YTTERBIUM DOPED SODIUM GADOLINIUM TUNGSTATE

The ultraviolet (UV) and infrared (IR) optical absorption (OA) edges of NaGdW were studied using a thin (78 μm) **a**-cut plate grown under the conditions Cz1. It was found that the UV band edge (roughly 4.2 eV at 5 K for both polarizations) is only weakly dependent on the temperature, see Fig. 2. The two weak bands at 306.3 and 312 nm, which can be seen in the same figure, correspond to the $^6P_{5/2}$ and $^6P_{7/2}$ ground state absorption of Gd^{3+}, respectively. The host transparency extends in the mid-IR up to about 5000 nm, see Fig. 2(a).

We also measured the refractive indices of Yb:NaGdW from the UV to the near-IR by the minimum deviation angle method using properly oriented prisms. Refractive indices have been previously reported only for three wavelengths in the visible and $x=0.015$ Yb.[24] Here we studied the room temperature dispersion and birefringence of undoped NaGdW and Yb:NaGdW with 18 mol % Yb in the crystal, both grown under Cz1 conditions. Both turned out to be positive crystals. It is worth noting that the ordinary refractive index n_o was found to be independent of the Yb^{3+} concentration, while the extraordinary refractive index n_e increases with the Yb content in the red and IR. The results were fitted to single-pole Sellmeier equations: $n^2=A$
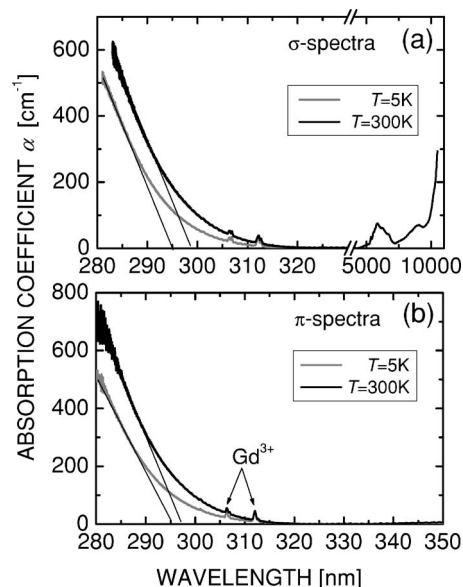

FIG. 2. Temperature dependence of the absorption coefficient α of NaGdW near the UV band edge for the two polarizations σ (a) and π (b). The unpolarized IR spectrum recorded at room temperature is included in (a).
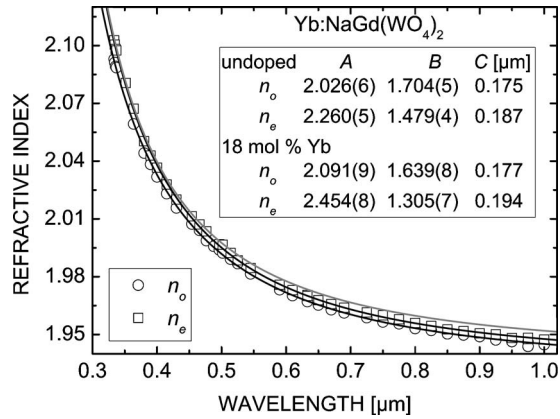
FIG. 3. Refractive indices of NaGdW measured at 300 K, $\mathbf{E} \perp \mathbf{c}$ (n_o, ○), $\mathbf{E}\|\mathbf{c}$ (n_e, □), with black curves representing our Sellmeier fits. For Yb:NaGdW, the behavior of n_o was very similar; the gray curve is the calculated Sellmeier fit obtained for n_e in this case (the experimental data are not shown for clarity).

$+B\lambda^2/(\lambda^2-C^2)$, where C corresponds to the UV pole. The parameters A, B, and C obtained from the fits are summarized in Fig. 3. The birefringence of the Yb:NaGdW crystals is rather low. This situation is similar to that found in NaLa(WO$_4$)$_2$ (Ref. 7) while the birefringence of NaBi(WO$_4$)$_2$ is much larger.[25]

Only brief and unpolarized Raman studies are known for NaGdW and they were performed with polycrystalline samples.[26] The strongest Raman peak of the stretching vibration of the $[\mathrm{WO_4}]^{2-}$ anion, the $\nu_1(A_1)$ mode according to the scheelite $I4_1/a$ symmetry, was found at 919 cm^{-1} in NaGdW.[26] This line of NaGdW is known for its potential for stimulated Raman scattering.[27] We measured polarized Raman spectra at room temperature with single crystals of low-doped Yb:NaGdW (Fig. 4) for better comparison with other related tungstates with ordered or disordered structure as well as for identification of the phonon bands in the low temperature absorption/emission spectra of Yb^{3+}. The excitation was at 488 nm with an Ar-ion laser and the scattered light was dispersed in a Jobin-Yvon spectrometer and de-
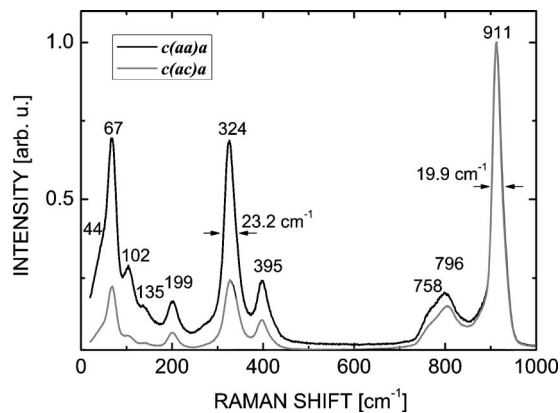

FIG. 4. Polarized Raman spectra recorded with single crystals of Yb:NaGdW with 1 mol % Yb doping grown under Cz2 conditions. The standard Porto notations designate the propagation/polarization configurations used for excitation and detection.

tected with a S1 photomultiplier. The strongest line was found in our measurements at 911 cm^{-1} and in contrast to Ref. 26 we did not observe any structuring of this line in the polarized spectra. Thus, the structure observed in Ref. 26 is maybe due to some inhomogeneous splitting caused by defects. The FWHM of the main peak (see Fig. 4) was slightly broader than the previously reported 14 cm^{-1} (Ref. 27) and 16 cm^{-1} (Ref. 26). The calculated dephasing time is 0.53 ps and this value is 3–4 times shorter than in the monoclinic double tungstates KT(WO$_4$)$_2$ (T=Gd, Y, Yb).[27] The difference is even larger if we compare with ordered tetragonal tungstates with scheelite structure (PbWO$_4$, CaWO$_4$, SrWO$_4$, BaWO$_4$).[26,27] Hence NaGdW is more suitable for operation with shorter pulses (e.g., 10 ps) maintaining the stationary regime of stimulated Raman scattering. Note that the observed FWHM in NaLa(WO$_4$)$_2$ and NaY(WO$_4$)$_2$ is similar.[26,27] The factor group analysis and the classification of the phonon frequencies for the $I\bar{4}$ symmetry can be found, e.g., in Ref. 19 where this SG was assigned to NaBi(WO$_4$)$_2$. The peak positions in Fig. 4 are also found in the Raman spectra of NaBi(WO$_4$)$_2$.

Finally, comparing with Fig. 2(a) one can conclude that the mid-IR absorption edge is preceded by two-phonon absorption which sets a practical long-wave limit for the transparency of NaGdW similar to previous observations in NaBi(WO$_4$)$_2$.[28]

IV. SPECTROSCOPIC PROPERTIES OF Yb^{3+} IN NaGdW

The optical electronic transition for the 4f^{13} configuration of Yb^{3+} can be partially magnetic-dipole (MD) allowed and three spectra have to be measured in general for a complete description of such uniaxial crystals: α ($\mathbf{E}\perp\mathbf{c}, \mathbf{H}\perp\mathbf{c}$), π ($\mathbf{E}\|\mathbf{c}$) and $\sigma(\mathbf{H}\|\mathbf{c})$. Several recent publications were devoted to the spectroscopy of Yb^{3+} in NaGdW.[29–32] The first measurements of the absorption and fluorescence of Yb^{3+} in NaGdW were unpolarized and at 300 K.[31] Polarized measurements at room temperature of a Yb:NaGdW sample with 1.5 mol % Yb in the crystal yielded peak absorption cross sections σ_{ABS} near 973 nm of $1.6\cdots1.7\times10^{-20}$ cm^2 (π polarization) and $1.2\cdots1.3\times10^{-20}$ cm^2 (σ polarization).[30,32] The emission cross sections σ_{EMI} were estimated in the same works by the Füchtbauer-Ladenburg formula with 320 μs as a value for the radiative lifetime τ_{RAD}. The maximum σ_{EMI} obtained for $\mathbf{E}\|\mathbf{c}$ near 996 nm was of the order of $1.7\cdots2\times10^{-20}$ cm^2 but the results for the σ polarization were obviously controversial. While in Ref. 29 the same authors reported roughly 20% higher maximum σ_{ABS} with a main peak at 976 nm, the more interesting observation in that work was that the main peak for the σ polarization and all secondary peaks for both polarizations depend on the Yb^{3+}-doping level in the range $1.3\cdots20$ mol % Yb in the crystal. This was attributed to increasing crystal disorder resulting from substitution of a large amount of Gd^{3+} ions by the smaller Yb^{3+} ions which, however, contradicts the conclusions of the same authors in their subsequent structural studies.[17,18] Spectroscopy of Yb^{3+} at low temperatures was not reported so far.

The quasi-three-level operation of ytterbium lasers depends on the crystal field splitting of the $^2F_{7/2}$ ground and
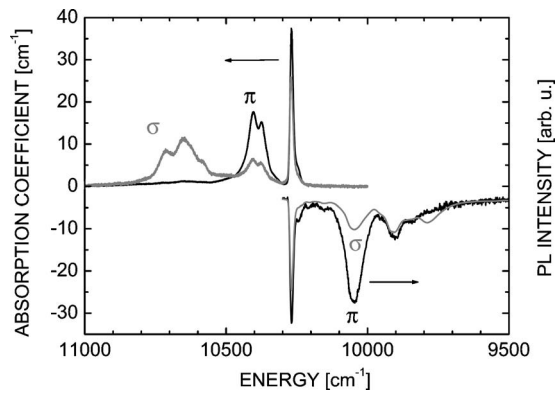
FIG. 5. Low temperature (5 K) spectroscopy of Yb:NaGdW for the π and σ polarizations. The absorption coefficient (left scale) is measured with a sample of 0.8 mol % Yb in the crystal and the photoluminescence (right scale) with a sample of 3.7 mol % Yb, excited at 961 nm.

$^2F_{5/2}$ excited manifolds. To quantify this effect the Yb^{3+} Stark levels have to be determined. Moreover, the possible spectral contributions of Yb^{3+} in different sites can be explored by low temperature spectroscopy. For these reasons we studied the 5 K OA and photoluminescence (PL) properties. For the OA studies we used samples of Yb:NaGdW with 3.7 and 8 mol % Yb in the crystal for which the results were identical. For the PL measurements we used samples with low Yb^{3+}-doping level, 0.8 and 3.7 mol % Yb in the crystal, and reflection geometry to minimize the reabsorption effect on the emission spectra. The PL was excited by a Ti:sapphire laser, dispersed in a Jobin-Yvon spectrometer and detected by a 77 K cooled Ge photodiode in conjunction with a lock-in amplifier.

Figure 5 shows the results of the 5 K OA measurements corresponding to the $^2F_{7/2}(0) \rightarrow {}^2F_{5/2}(n')$ electronic transitions. The simultaneously recorded α spectrum cannot be visually distinguished from the σ spectrum and is omitted for brevity. A well resolved band ($n'=0$) with a FWHM of about 13 cm^{-1} is observed in the OA spectra at 10 269 cm^{-1}. Such a linewidth is similar to those observed at low temperature (5 K) for the Ln transitions in other disordered double tungstates.[20] Two overlapping but still resolved bands ($n' = 1$) are observed at 10 404 and 10 375 cm^{-1}. In addition several overlapping bands ($n'=2$) in the 10 600–10 700 cm^{-1} range are observed only in the σ (and α) spectra.

In order to ascertain whether these spectral structures correspond to the two different Yb sites expected from the $I\bar{4}$ SG and the associated disordered character of their cationic environments or to vibronic couplings often observed for Yb^{3+},[33] we studied in detail the PL excitation and emission spectra. For this purpose the excitation wavelength, λ_{EXC}, was changed by steps of 1 nm within the line profile of the different overlapping peak groups ($\lambda_{EXC} = 10\,200-10\,295$ cm^{-1}, $10\,295-10\,515$ cm^{-1}, and $10\,515-10\,800$ cm^{-1}) and the emission was recorded for each λ_{EXC}. We observed that the shape and spectral position of the emission peaks change with λ_{EXC} and also that the corresponding excitation spectra depend on the detected wavelength, λ_{EMI}.
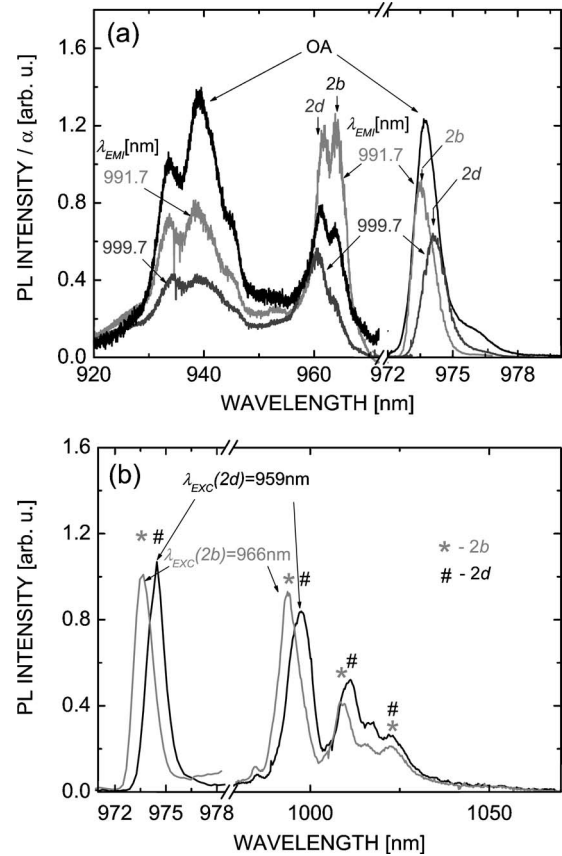

FIG. 6. Unpolarized PL spectra of Yb:NaGdW with 0.8 mol % Yb in the crystal recorded at 5 K: (a) Comparison of the excitation spectra at several emission wavelengths, λ_{EMI}, with the optical absorption (OA) where the absorption coefficient α is rescaled for clarity. (b) Emission spectra for selected excitation wavelengths, λ_{EXC}. 2b and 2d indicate the two crystallographic sites characteristic for the $I\bar{4}$ SG.

Figure 6 shows selected representative examples of these changes. It should be outlined that the excitation bands are equal in width or narrower than the OA bands and are lying within the latter, see Fig. 6(a).

These OA and PL spectra can be partially interpreted in terms of the two crystallographic sites for Yb^{3+} in the SG $I\bar{4}$ previously determined. For this purpose we applied the semi-empirical simple overlap model (SOM),[34] which allows to estimate the crystal field parameters (CFPs) from the crystallographic positions of the Gd(or Yb)O$_8$ coordination polyhedra. Separate sets of CFPs for the Yb^{3+} ions in the 2b and 2d sites were obtained from the atomic coordinates given in Table II and the corresponding Yb-O bond distances. The values of the 6 CFPs corresponding to the S_4 symmetry were introduced independently for each site in the simulation of the $^2F_{7/2}(n)$ and $^2F_{5/2}(n')$ Stark level energies for the $4f^{13}$ configuration, along with free ion (FI) parameters previously determined for the isostructural NaBi(WO$_4$)$_2$ host.[35] The simulation was performed using a previously developed code.[36] The used FI parameters, the derived SOM CFPs, and the corresponding energy level schemes obtained for Yb^{3+} in each of the two sites are summarized in Table III.

TABLE III. FI (E^0 and ζ) parameters and calculated SOM CFPs (B_0^2, B_0^4, B_4^4, B_0^6, B_4^6, and S_4^6) used to calculate the $^2F_{7/2}(n)$ and $^2F_{5/2}(n')$ energy levels of Yb^{3+} in the 2b and 2d sites of NaGdW. The experimentally determined energy levels are included in parentheses. All energies are relative to the $^2F_{7/2}(0)$ level for the corresponding site. Parameters and energies are given in cm^{-1}. Overlap between Yb ligand (oxygen) orbital wave functions: $\rho=0.08$, effective charge for oxygen: -1.

Site	2d	2b
E^0		4607.03
ζ	2908.00	2910.50
B_0^2	435	551
B_0^4	−674	−667
B_4^4	±634	±610
B_0^6	−31	−94
B_4^6	±287	±297
S_4^6	±337	±350
$^2F_{5/2}(2')$	10613 (10648)	10652 (10710)
$^2F_{5/2}(1')$	10381 (10411)	10366 (10373)
$^2F_{5/2}(0')$	10259 (10266)	10272 (10272)
$^2F_{7/2}(3)$	460 (482)	496 (492)
$^2F_{7/2}(2)$	287 (371)	281 (360)
$^2F_{7/2}(1)$	199 (239)	181 (209)
$^2F_{7/2}(0)$	0 (0)	0 (0)

The comparison of these calculated levels with the energies corresponding to the experimental OA bands permits to identify the individual contribution of the 2b and 2d sites to the $^2F_{7/2}(0) \rightarrow {}^2F_{5/2}(0',1')$ transitions of the Yb^{3+} ion. In particular, the different sequence experimentally found for the $^2F_{5/2}(0')$ and $^2F_{5/2}(1')$ levels in the two sites is well reproduced by the simulation. The obtained assignments are sketched in Fig. 7 and the bands are correspondingly labeled in Figs. 6(a) and 6(b). It is worth noting that the relative intensity of the $^2F_{7/2}(0) \rightarrow {}^2F_{5/2}(0',1')$ transitions labeled as 2b and 2d roughly corresponds to the Yb^{3+} OFs given in Table II. The separate site contributions to the $^2F_{7/2}(0)$
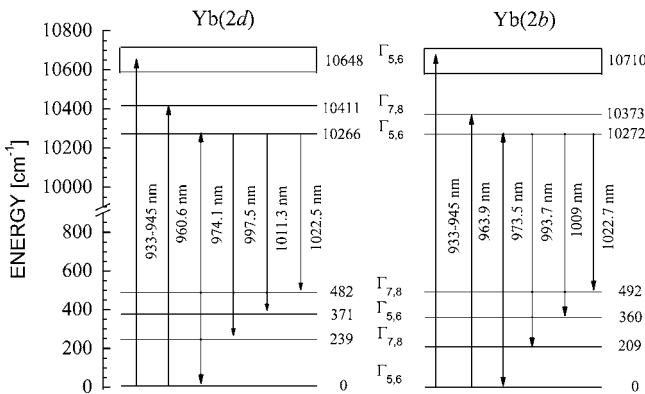

FIG. 7. Energy level scheme of Yb^{3+} in the 2b and 2d sites of the NaGdW host.

TABLE IV. Selection rules for electric dipole (ED) and magnetic dipole (MD) electronic transitions in the S_4 point symmetry group. $\Gamma_{5,6}$, $\Gamma_{7,8}$ are the two allowed irreducible representations for $J=5/2$ and $7/2$ in S_4.

S_4	ED		MD	
	$\Gamma_{5,6}$	$\Gamma_{7,8}$	$\Gamma_{5,6}$	$\Gamma_{7,8}$
$\Gamma_{5,6}$	α, σ	α, σ, π	α, σ, π	α, π
$\Gamma_{7,8}$	α, σ, π	α, σ	α, π	α, σ, π

$\rightarrow {}^2F_{5/2}(2')$ transitions were more difficult to identify since three or four OA bands are experimentally observed in the $10\,515-10\,800$ cm^{-1} spectral range, see Figs. 5 and 6(a). Nevertheless they were resolved with a similar experiment of selective excitation of the low temperature PL at 931 and 965 nm for the 2d site, and at 944 and 961 nm for the 2b site.

The energy difference between the $^2F_{7/2}$ levels (0) and (1) was initially estimated from the thermal evolution of the OA (not presented here for the sake of brevity)—about 218 cm^{-1}. A more precise evaluation of the energy positions of the $^2F_{7/2}(n)$ Stark energy levels for each site was inferred from the 5 K PL spectra under selective excitation shown in Fig. 6(b). The level energies obtained are summarized in Fig. 7 and Table III. The crystal field splitting in NaGdW is similar to that found in other Yb^{3+}-doped disordered DT laser hosts[7] and comparable to the splitting in the ordered monoclinic KY(WO$_4$)$_2$ and KGd(WO$_4$)$_2$.[37]

The crystal field calculations presented above have determined the irreducible representations of the $^2F_{7/2}(n)$ and $^2F_{5/2}(n')$ Stark levels as specified in Fig. 7. Table IV presents the expected selection rules for Yb^{3+} in S_4 symmetry. As a first approximation the experimental $^2F_{7/2}(0) \rightarrow {}^2F_{5/2}(n')$ bands can be classified as α, σ, π; α, σ, π and α, σ, for $n'=0',1',2'$ respectively. To make this consistent with the expected transition selection rules, a partial magnetic dipole character of the $0 \rightarrow 0'$ transition should be assumed.

The measurements of the OA at 5 K of Yb:NaGdW with 8 mol % Yb in the crystal grown under Cz1 conditions, indicated identical absorption coefficient for the α and σ polarizations (Fig. 5). The α spectrum remains quite similar to the σ spectrum also at room temperature.[4] We performed analogous measurements on a sample grown under Cz3 conditions with 3.7 mol % Yb in the crystal and a sample grown under Cz2 conditions with 20 mol % Yb in the crystal, and obtained quite similar results, see Fig. 8. The maximum σ_{ABS} near 975 nm amounts to 1.78 and 1.36×10^{-20} cm^2 for the π and σ polarizations, respectively. These values are very close to earlier measurements.[30,32] The results shown in Fig. 8 together with the polarized room temperature PL measurements were used to calculate the emission cross sections (shown in the same figure) by a combination of the reciprocity and Füchtbauer-Ladenburg methods. The maximum σ_{EMI} for the π polarization amounts to 1.89×10^{-20} cm^2 near 1000 nm. This value is roughly six times lower than the maximum σ_{EMI} in monoclinic potassium double tungstates which are characterized by much stronger anisotropy.[38]
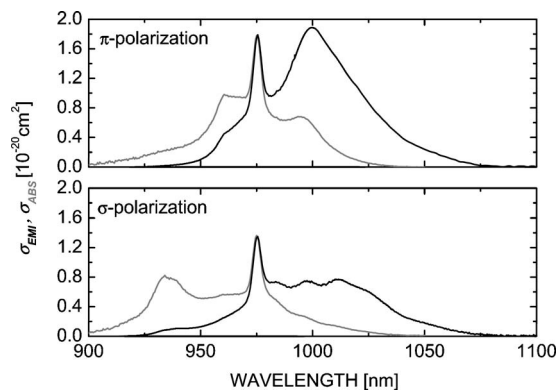
FIG. 8. Absorption cross section σ_{ABS} of Yb:NaGdW measured at room temperature (gray curves) and calculated emission cross sections σ_{EMI} (black curves) for the π and σ polarizations. A 0.452 mm thick sample with 20 mol % Yb in the crystal grown under Cz2 conditions was used for the absorption measurements.

Since ytterbium lasers operate as a quasi-three-level system the emission spectra are not sufficient to predict which of the polarizations exhibits higher gain. This can be determined by calculating the gain cross section according to $\sigma_{GAIN}(\lambda) = \beta \sigma_{EMI}(\lambda) - (1-\beta)\sigma_{ABS}(\lambda)$, where β denotes the ratio of the inverted ions to the total Yb^{3+}-ion density. The results are shown in Fig. 9. They substantially differ from the gain spectra presented in previous works,[30,32] and predict, in contrast, higher gain for the π polarization. This will be confirmed by the laser results presented in the next section.

Previous measurements of fine powders of Yb:NaGdW in an immersion liquid yielded 320 μs for the $^2F_{5/2}$ fluorescence decay time, independent of the Yb^{3+}-doping level in the 0.5…5 mol % range for the ground crystals.[30,32] The same authors obtained a radiative lifetime of $\tau_{RAD} = 397$ μs calculated from the absorption spectra.[32] We performed extensive lifetime measurements on several samples, including heavily doped, both with the powder and the pinhole methods which are not affected by radiation trapping. The 320 μs value was reproduced both at low doping levels and in the heavily doped samples. The radiative lifetime calculated from the emission cross section data in Fig. 8 using $1/\tau_{RAD} = 8\pi n^2 \int \langle \sigma_{EMI}(\nu) \rangle / (\lambda^2) d\nu$,[38] where the averaging is over the polarization, amounts to 480 μs.
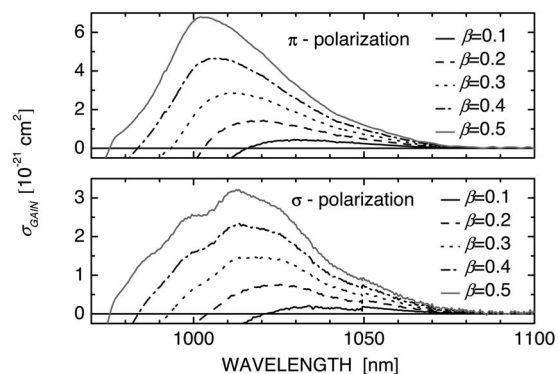

FIG. 9. Calculated gain cross section σ_{GAIN} of Yb:NaGdW for different inversion ratios β.

V. LASER EXPERIMENTS AND RESULTS

The laser experiments described in this section were performed with two uncoated samples of Yb:NaGdW cut from the same boule grown under Cz3 conditions with $x = 0.13$. The doping level determined by the microprobe analysis method, 10.74 mol %, gives an Yb^{3+} density of 6.87 $\times 10^{20}$ cm^{-3} in the crystal. The Yb^{3+} concentration determined by laser absorption measurements using the cross sections from Fig. 8 was rather consistent, 6.46×10^{20} cm^{-3}. Sample A was **a**-cut and 3.3 mm thick with an aperture of 6×5 mm^2. This sample could be used exactly both for the π and the σ polarizations under normal incidence or approximately, when inserted under Brewster angle. Sample B was 1.1 mm thick and had an aperture of 9×12 mm^2. It was **c**-cut, hence it could be used only for the σ polarization. Visually both samples seemed to have perfect quality (no inclusions or striations) and from the laser experiments it was possible to conclude that they are rather homogeneous.

Longer cavities with folded focusing sections are important for achievement of tunable laser operation and passive mode locking because they can be easily extended to include additional elements. The astigmatically compensated three-mirror cavity shown in Fig. 10(a) was first studied with Ti:sapphire laser pumping using sample A. The total physical cavity length was 73.4 cm. Both M_1 and M_2 were highly transmitting for the pump radiation which ensured single pass longitudinal pumping and helped to avoid any feedback to the pump laser. Both the rear sides of these mirrors and the $f = 62.8$ mm pump lens L were antireflection coated and introduced only negligible reduction of the pump power so that
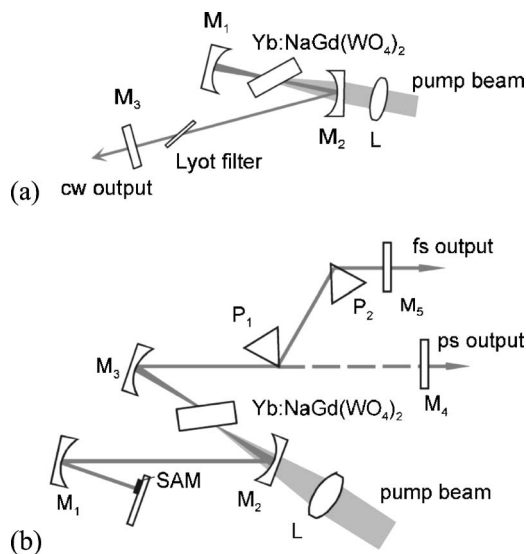

FIG. 10. Astigmatically compensated three-mirror cavity with Brewster geometry and an intracavity tuning element (a), and its extension for passive mode locking (b). In (a): M_1 and M_2: total reflectors for the laser radiation with radius of curvature (RC) equal to −50 mm and −100 mm, respectively, M_3: plane output coupler. In (b): M_1, M_2, and M_3: total reflectors for the laser radiation with RC=−150 mm, −100 mm, and −100 mm, respectively, M_4 and M_5: plane output couplers, P_1 and P_2: Brewster prisms, SAM: saturable absorber mirror.

the power incident onto the crystal, P_{INC}, could be conveniently measured outside the resonator. A two-plate Lyot filter could be inserted in the vicinity of the output coupler M_3 for tuning.

The pump and the laser spot diameters were almost equal in the position of the crystal and we estimated from the Brewster reflection a Gaussian pump waist of $w_P \approx 22$ μm. Thus the pump beam size was $\pi w_P^2/2 = 7.6 \times 10^{-6}$cm^2. The peak incident on-axis intensity for the maximum $P_{INC} = 2$ W used in this experiment was 260 kW/cm^2. Averaging over the beam cross section by taking a factor of 0.5 means that the pump intensity exceeds approximately 3.6 times (π) and 2.8 times (σ) the saturation intensity. For both polarizations, however, our measurements showed that at high pump levels the absorption bleaching effect is cancelled to a great extent by the increase of the actual saturation intensity caused by the circulating intracavity power which is a typical effect for a three level laser system (Fig. 11). It should be outlined that the bleaching effect, as can be seen from Fig. 11, is weaker in comparison with our initial results obtained at a lower doping level.[4]

The input-output characteristics shown in Fig. 12 indicate a substantial improvement in comparison with the results obtained at lower Yb^{3+}-doping levels.[4] The slope and optical pump efficiencies, as well as the output power levels, are roughly three times higher. This is associated, however, not only with the increased concentration of Yb^{3+} ions but to a greater extent with the improved optical quality because the thresholds did not increase at the higher doping level. The π polarization yielded slightly better results which can be attributed, having in mind the very similar absorbed powers, to the higher gain cross section (Fig. 9) but in general the behavior which depends on the self-adjusting lasing wavelength is quite similar for the two polarizations. The lasing wavelength λ_L is influenced by reabsorption and due to the higher doping is increased now in comparison to experiments with lower doping.[4] The optimum pump wavelengths λ_P indicated in Figs. 11 and 12 are very close to the absorption maxima of the corresponding spectra (Fig. 8). Thermal effects were not observed up to the maximum $P_{INC} = 2$ W applied although no special cooling was provided to the Yb:NaGdW crystal.

In view of the mode-locking potential, it was interesting to study the same laser configuration also with diode pumping and in this case a 2 W polarized tapered diode laser (TDL) of nearly diffraction limited beam quality (M^2 value for the slow axis emission <3) was employed; more information on this TDL can be found elsewhere.[39] It required only simple forming optics and could be used directly with the cavity setup shown in Fig. 10(a). Both pump and laser polarizations were π. The results obtained with two different output couplers are shown in Fig. 13. The reduced slope efficiencies can be attributed to the worse mode matching but they are still rather high for diode pumping.

Tuning was studied with the same cavity configuration using sample A and inserting the Lyot filter, only for Ti:sapphire laser pumping. Under optimum alignment the output power reduction with the filter inside the cavity did not exceed 10%. The obtained results are shown in Fig. 14. As could be expected, the improved laser efficiency allowed to
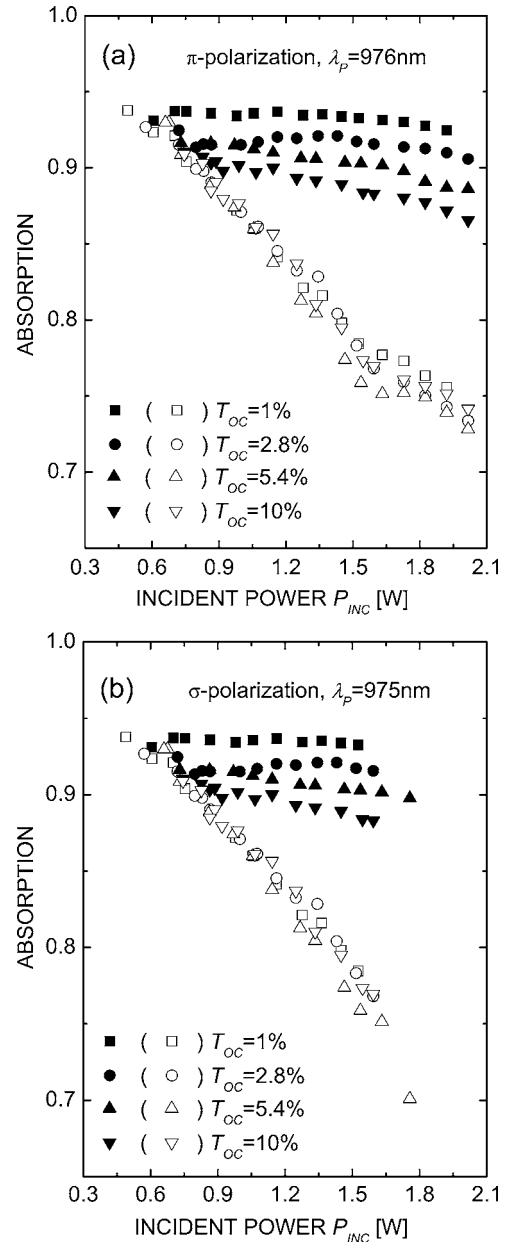

FIG. 11. Measured single pass absorption of the Yb:NaGdW sample A with lasing (full symbols) and with lasing interrupted in the arm containing the output coupler (open symbols), versus incident pump power P_{INC} for several output couplers. The nonlasing data should be independent of T_{OC} and the four data sets are indicative of the precision of this measurement.

extend the achievable tunability ranges by roughly 50% in comparison to our previous studies.[4] The full tunability achieved for the π polarization extends from 1014 to 1079 nm. The laser did not operate at longer wavelengths with the 1% output coupler. This can be explained by the fact that the losses introduced by the tuning element push the laser operation to shorter wavelengths (as can be seen from the T_{OC}=5.4% curve) which is not compatible with the filter alignment. This effect has, however, no relevance to mode-locked operation. Provided the bandwidths recorded in Fig. 14 could be fully utilized, the FWHM of more than 12 THz
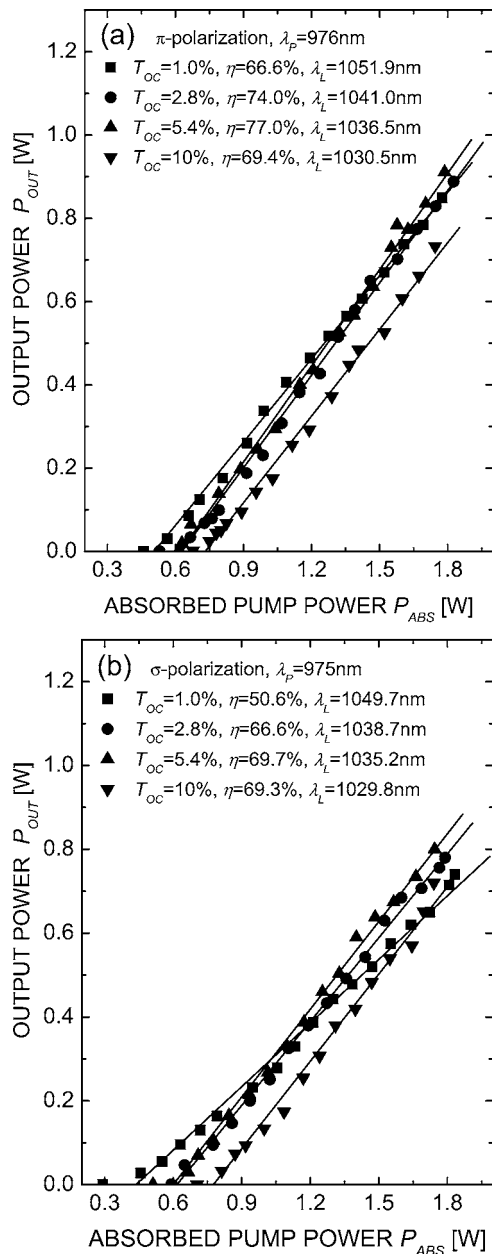
FIG. 12. Output power P_{OUT} versus absorbed pump power P_{ABS} (symbols) for the three-mirror Yb:NaGdW laser with Ti:sapphire laser pumping and linear fits (lines) for calculation of the slope efficiency η for four different output couplers (T_{OC}).

for the π polarization means that the lower theoretical limit for the achievable pulse duration with passive mode locking of this laser is less than 50 fs.

For mode locking we used the Z-shaped astigmatically compensated cavity depicted in Fig. 10(b) and the same Yb:NaGdW sample A was positioned under Brewster angle between the two folding mirrors. Two SF10 Brewster prisms separated by 32.5 cm could be inserted into the arm with the output coupler for dispersion compensation and the other arm contained a third focusing mirror to produce an additional waist on the semiconductor saturable mirror (SAM). The Ti:sapphire laser pump beam was focused by the same f=62.8 mm lens L. Without the intracavity prisms [see Fig.
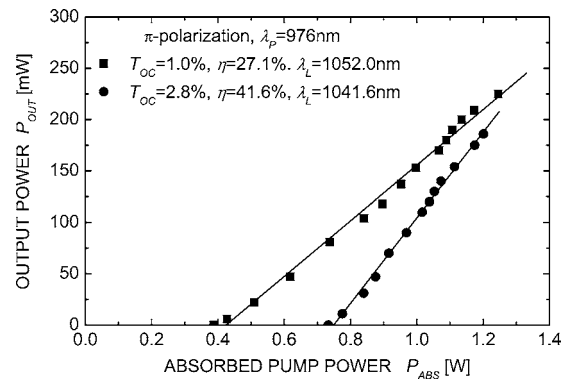

FIG. 13. Output power P_{OUT} versus absorbed pump power P_{ABS} (symbols) of the CW Yb:NaGdW laser obtained with TDL pumping using a three-mirror cavity, and linear fits (lines) for calculation of the slope efficiency η for two different output couplers (T_{OC}).

10(b)] this laser operated in the picosecond regime, passively mode locked and self-starting with the SAM. With the two prisms inside the cavity, femtosecond mode-locked operation was achieved. The physical cavity length of 155 cm corresponded in this case to a pulse repetition rate of roughly 97 MHz. At an incident pump power of P_{INC}=1.8 W, the output power reached P_{OUT}=360 mW for T_{OC}=2.8%. The crystal absorption in the lasing state was 76% which gives an efficiency of roughly 26% in the mode-locked regime. The autocorrelation trace shown in Fig. 15(a), recorded by second harmonic generation, corresponds to a pulse duration
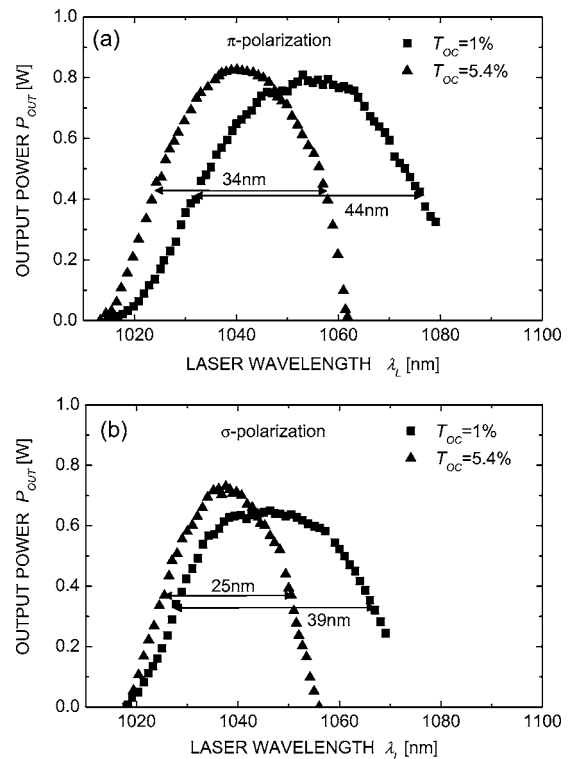

FIG. 14. Output power P_{OUT} versus laser wavelength λ_L for an incident pump power of P_{INC}=2.0 W (Ti:sapphire laser pumping). The crystal orientation corresponds to π polarization (a) with λ_P=976 nm and σ polarization (b) with λ_P=975 nm.
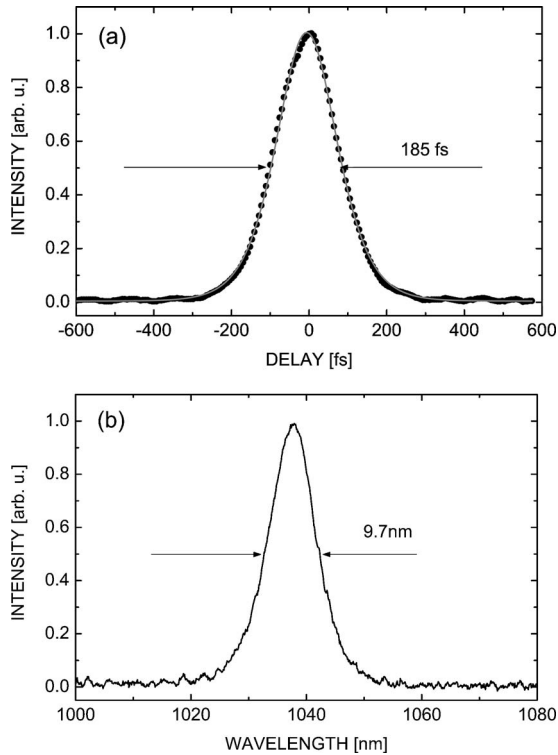
FIG. 15. Autocorrelation trace (a) and spectrum (b) of the femtosecond Yb:NaGdW laser. The symbols in (a) are the experimental points while the fit is shown by the curve.

FIG. 16. Output power P_{OUT} and crystal absorption versus absorbed pump power P_{ABS} of the CW Yb:NaGdW laser pumped by the unpolarized diode in a single pass. The linear fits (lines) were used for calculation of the slope efficiency η for different output couplers (T_{OC}).

(FWHM) of 120 fs assuming a sech[2]-pulse shape as shown by the fit. The simultaneously recorded spectrum, Fig. 15(b), is centered at 1037.5 nm and has a FWHM of 9.7 nm. This gives a time-bandwidth product of 0.324, which is extremely close to the Fourier limit for the assumed pulse shape, 0.315.

We believe that the use of a more appropriate SAM or direct Kerr-lens mode locking will allow to reduce the pulse duration from this laser in the near future to below 50 fs. This is supported by the observation of sub-80 fs pulse durations at lower doping levels, however, the realization of this regime occurred at shorter laser wavelengths which requires special cavity optics for optimization and stabilization.[40]

In order to evaluate the power scaling capabilities of the laser with diode pumping we studied also simple planoconcave hemispherical cavities consisting of only two mirrors. Sample A, mounted in a Cu ring but without active cooling, was studied in a linear cavity containing an output coupler with RC=−50 mm which was highly transmitting at λ_P, i.e., the pumping was in a single pass. The pump source was an unpolarized 8 W fiber-coupled diode module (116 μm core diameter and NA=0.2 at the fiber output) consisting of 6×2 W diodes with 100 μm emitters (Boston Laser, Inc.). The $f=6.2$ mm microfocusing optics (Schäfter&Kirchhoff) had a working distance of 3.5 mm in air or about 5 mm through the 3 mm thick quartz substrate of the incoupling plane mirror. The Gaussian waist in the focus was $w_P=40$ μm, the Rayleigh length $Z_R=0.36$ mm, and the confocal length (depth of focus) $b=2Z_R=0.72$ mm. These parameters which were measured in air correspond to
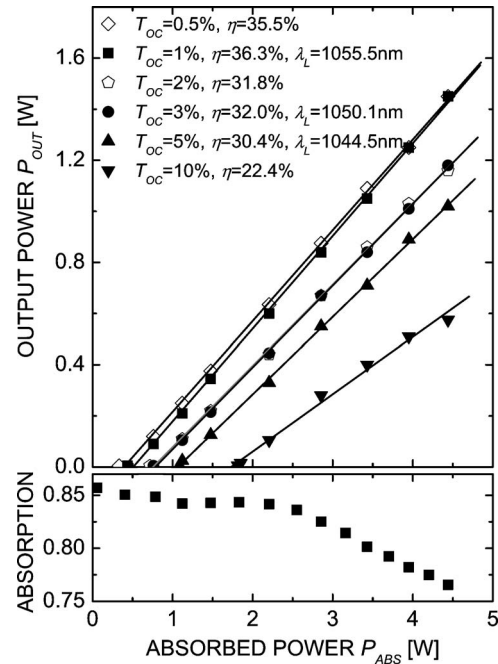
$M^2=14$. The transmission of the incoupling mirror at the pump wavelength was 97%. We measured the incident pump power P_{INC} behind it, i.e., in front of the sample. In the laser experiment, however, the Yb:NaGdW sample was very close (0.2 mm) to this mirror.

The CW laser characteristics obtained are shown in Fig. 16 versus absorbed pump power P_{ABS}. The latter was calculated subtracting from P_{INC} the measured transmitted pump power. Hence the increase of the pump saturation intensity due to the circulating intracavity intensity was not taken into account because power measurements of the highly divergent pump were possible only in the nonlasing state (output coupler removed). Nevertheless, the fact that the inputoutput characteristics looked very similar when plotted against P_{INC} is an evidence for the weakness of this effect. The slope efficiencies calculated with respect to P_{INC} were 75–76% ($T_{OC}=0.5$–5%) and $\approx72\%$ ($T_{OC}=10\%$) of those shown in Fig. 16 against P_{ABS}. The measurements with the output coupler removed indicate an absorption decrease with the pump power from 0.857 to 0.766 (Fig. 16). It can be expected that the intracavity laser intensity balances this effect and in that case an average absorption of 84% can be assumed for the whole range. Using this value as a correction factor (i.e., assuming $P_{ABS}=0.84P_{INC}$), one obtains, e.g., for $T_{OC}=1\%$, $\eta=33\%$ which is indeed a small difference from the value given in Fig. 16. In reality, the situation is much more complicated since the pump diode spectrum is multipeaked and changes with the power.

In the absence of polarization selection in this linear cavity with the **a**-cut sample the laser output was always π polarized due to the higher gain. This is a direct confirmation
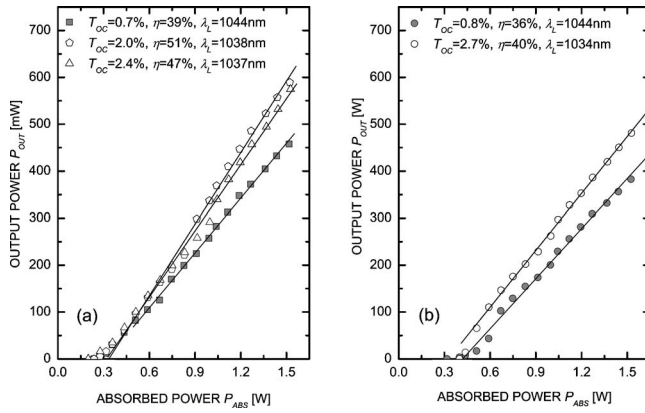
FIG. 17. Output power P_{OUT} versus absorbed pump power P_{ABS} of the CW Yb:NaGdW laser pumped by the polarized diode in a double pass with an output coupler having RC=−100 mm (a) and −50 mm (b). The linear fits (lines) were used for calculation of the slope efficiency η for different output couplers (T_{OC}).

of the higher gain cross section for this polarization (Fig. 9). Maximum output powers P_{OUT} of 1.45, 1.18, and 1.02 W were obtained with T_{OC}=1, 3, and 5%, respectively. T_{OC} =0.5 and 1% led to very similar results, the results were close also for T_{OC}=2 and 3% while the mirror with T_{OC} =10% gave the lowest slope efficiency with a maximum P_{OUT} of only 0.575 W. The laser wavelength λ_L measured slightly above threshold was 1052.7, 1045.9, and 1041.5 nm for T_{OC}=1, 3, and 5%, respectively, i.e., only slightly lower than the values measured at maximum P_{OUT} given in Fig. 16. This indicates that the actual crystal absorption changes little with P_{INC} and that thermal effects are only weak. The latter is also clear from the fact that no rollover can be seen in the recorded power dependences. This is an important prerequisite for further power scaling because the measurement of the thermal conductivity of Yb:NaGdW (x=0.05) performed recently,[13] indicates moderate values: ≈ 1.1 W m^{-1} K^{-1} along the **a** and ≈ 1.2 W m^{-1} K^{-1} along the **c** axis.

Using Sample B in a similar hemispherical linear cavity it was possible to improve substantially (roughly two times in terms of output power and efficiency) also our preliminary results obtained with a polarized pump diode using lower Yb doping.[5] In this case the sample was mounted on a water cooled Cu block and placed also as close as possible to the incoupling plane mirror through which the pump beam was focused by an f=30 mm lens. The 3-W laser diode pump source (Unique Mode UM 3000/M10/CB) operated near 975 nm and had M^2=10. The pump laser was isolated by a Faraday rotator. Double-pass pumping was applied in order to increase the absorbed pump power. This was possible through the output couplers which reflected also the pump radiation. This **c**-cut sample was pumped by linearly polarized light but the laser output was unpolarized although both pump and laser polarizations were perpendicular to the crystal **c** axis.

For comparison the results in Fig. 17 are presented against the absorbed pump power: Both pump passes were taken into account using the absorption measured in the nonlasing state near the threshold, i.e., assuming a constant absorption which should be roughly true as clear from the above discus-

sion of the bleaching effects. The lower thresholds and higher slope efficiencies obtained in this case in comparison to Fig. 16 are related to the better mode matching with the higher quality pump beam. The laser wavelength varied between 1025 and 1044 nm depending on the output coupler used.

VI. SUMMARY

NaGd(WO$_4$)$_2$ crystals doped with up to 20 mol % Yb^{3+} can be grown free of defects with dimensions as large as 40 cm^3 by the Czochralski method. When these crystals are cooled to room temperature at slow (4−10 °C/h) or moderate (80 °C/h) rates they exhibit at 300 K the $I\bar{4}$ crystalline symmetry without inversion center. In this symmetry there are two sites, $2b$ and $2d$, shared by Na$^+$ and Gd^{3+}/Yb^{3+} cations with specific occupancy factors. These crystals are Na deficient due to evaporation from the melt and correspondingly have an excess of trivalent cations (Gd^{3+} and Yb^{3+}). The latter occupy preferentially the $2b$ site, typically 60–65% versus 45–40% in the $2d$ site.

These two crystalline sites have the same S_4 local symmetry but different sets of Yb-O distances, i.e., different crystal fields. Moreover, each site is characterized by several environments due to the different Na-Gd/Yb cationic distributions in the first cationic sphere. The energy levels of Yb^{3+} have been resolved by 5 K optical spectroscopy and assigned to a specific site by comparison with the $^2F_{5/2}$ or $^2F_{7/2}$ Stark level positions calculated using the crystal field parameters obtained by the simple overlap model (using the Yb and O lattice positions) along with the free ion parameters from the literature. The optical spectroscopy of Yb^{3+} shows polarization features consistent with the S_4 local symmetry and a non-negligible magnetic dipole contribution to the $^2F_{7/2}(0) \leftrightarrow {}^2F_{5/2}(0')$ transition.

The transparency range of NaGdW defined at 1 cm^{-1} extends from 0.32 to 4.5 μm; within this range the crystal is positive uniaxial ($n_o < n_e$) with weak birefringence ($\Delta n < 0.01$). The most intense optical phonons are at 67, 324, and 911 cm^{-1}. Some of the physical properties have been found to depend on the Yb^{3+} concentration, e.g., the extraordinary refractive index increases with the Yb content while the ordinary one remains unaffected. The maximum Yb absorption cross section, σ_{ABS}=1.78×10^{-20} cm^2, was measured at 975 nm for the π polarization. This main peak has a FWHM$\approx$7 nm. The largest emission cross section, σ_{EMI} =1.89×10^{-20} cm^2 at 1000 nm, was obtained also for the π polarization. The gain cross section is higher for the π polarization, which was confirmed in the laser experiments.

CW Yb^{3+}-laser operation in NaGdW was studied at room temperature both under Ti:sapphire and diode laser pumping. Maximum slope efficiency of 77% with respect to the absorbed power was achieved for π polarization with Ti:sapphire laser pumping using a three-mirror cavity and Brewster geometry. The emission was tunable in the 1014−1079 nm spectral range with an intracavity Lyot filter. The FWHM of more than 12 THz achieved for the π polarization is expected to support <50 fs pulses in passively mode-locked

laser operation. The experimental realization of this regime using SAM and two intracavity prisms yielded 120 fs long output pulses at an average power of 360 mW and a repetition frequency of ≈ 97 MHz. The use of diode pumping with simple two mirror cavities produced an output power as high as 1.45 W and the maximum slope efficiency was 51%.

ACKNOWLEDGMENTS

*Email address: petrov@mbi-berlin.de

[1] V. K. Trunov, V. A. Efremov, and J. A. Velikodnyj, *Kristallochimija i svojstva dvojnych molibdatov i vol'framatov* (Nauka, Leningrad, 1986), in Russian.

[2] G. E. Peterson and P. M. Bridenbaugh, Appl. Phys. Lett. **4**, 173 (1964).

[3] N. Faure, C. Borel, M. Couchaud, G. Basset, R. Templier, and C. Wyon, Appl. Phys. B: Lasers Opt. **63**, 593 (1996).

[4] M. Rico, J. Liu, U. Griebner, V. Petrov, M. D. Serrano, F. Esteban-Betegón, C. Cascales, and C. Zaldo, Opt. Express **12**, 5362 (2004).

[5] J. Johannsen, M. Mond, K. Petermann, G. Huber, L. Ackermann, D. Rytz, and C. Dupre, Advanced Solid-State Photonics 2005, Feb. 6–9, 2005, Vienna, Austria, Technical Digest, CD ROM, paper MB44.

[6] J. Liu, J. M. Cano-Torres, C. Cascales, F. Esteban-Betegón, M. D. Serrano, V. Volkov, C. Zaldo, M. Rico, U. Griebner, and V. Petrov, Phys. Status Solidi A **202**, R29 (2005).

[7] J. Liu, J. M. Cano-Torres, F. Esteban-Betegón, M. D. Serrano, C. Cascales, C. Zaldo, M. Rico, U. Griebner, and V. Petrov, Opt. Laser Technol. **39**, 558 (2007).

[8] M. Rico, J. Liu, J. M. Cano-Torres, A. García-Cortés, C. Cascales, C. Zaldo, U. Griebner, and V. Petrov, Appl. Phys. B: Lasers Opt. **81**, 621 (2005).

[9] A. V. Mandrik, A. E. Troshin, V. E. Kisel, A. S. Yasukevich, G. N. Klavsut, N. V. Kuleshov, and A. A. Pavlyuk, Appl. Phys. B: Lasers Opt. **81**, 1119 (2005).

[10] M. Rico, U. Griebner, V. Petrov, P. Ortega, X. Han, C. Cascales, and C. Zaldo, J. Opt. Soc. Am. B **23**, 1083 (2006).

[11] V. Petrov, M. Rico, J. Liu, U. Griebner, X. Mateos, J. M. Cano-Torres, V. Volkov, F. Esteban-Betegón, M. D. Serrano, X. Han, and C. Zaldo, J. Non-Cryst. Solids **352**, 2371 (2006).

[12] H. Wang, G. Jia, F. Yang, Y. Wie, Z. You, Y. Wang, J. Li, Z. Zhu, X. Lu, and C. Tu, Appl. Phys. B: Lasers Opt. **83**, 579 (2006).

[13] J. Fan, H. Zhang, J. Wang, Z. Ling, H. Xia, X. Chen, Y. Yu, Q. Lu, and M. Jiang, J. Phys. D **39**, 1034 (2006).

[14] M. V. Mokhosoev, V. I. Krivobok, S. M. Aleikina, N. S. Zhigulina, and N. G. Kisel', Izv. Akad. Nauk SSSR, Neorg. Mater. **3**, 1657 (1967) [Inorg. Mater. **3**, 1444 (1967)].

[15] E. Ya. Rode, V. N. Karpov, and M. M. Ivanova, Zh. Neorg. Khim. **16**, 1713 (1971) [Russ. J. Inorg. Chem. **16**, 905 (1971)].

[16] JCPDS-card 25–0829. McIlvried, McCarthy (1973).

[17] E. V. Zharikov, G. M. Kuz'micheva, D. A. Lis, Yu. M. Papin, V. B. Rybakov, B. A. Smirnov, and K. A. Subbotin, Neorg. Mater. **39**, 200 (2003) [Inorg. Mater. **39**, 151 (2003)].

[18] G. M. Kuz'micheva, D. A. Lis, K. A. Subbotin, V. B. Rybakov, and E. V. Zharikov, J. Cryst. Growth **275**, e1835 (2005).

[19] J. Hanuza, A. Benzar, A. Haznar, M. Maczka, A. Pietraszko, and J. H. Van der Maas, Vib. Spectrosc. **12**, 25 (1996).

[20] C. Cascales, A. Méndez-Blas, M. Rico, V. Volkov, and C. Zaldo, Opt. Mater. **27**, 1672 (2005).

[21] SHELXTL Version 6.10 software package, Siemens Energy and Automation, Inc., Analytical Instrumentation.

[22] R. C. T. Slade, B. C. West, and G. P. Hall, Solid State Ionics **32/33**, 154 (1989).

[23] J. Sadanandam and S. V. Suryanarayana, Nat. Acad. Sci. Lett. **2**, 195 (1979).

[24] М. Голубьев and С.Ульянов, "Investigation of the dispersive properties of double tungstates $NaGd(WO_4)_2$, activated with Yb^{3+} ions," http://abitu.ru/start2/closed/viewwork.html?work=47, in Russian.

[25] V. Volkov, M. Rico, A. Méndez-Blas, and C. Zaldo, J. Phys. Chem. Solids **63**, 95 (2002).

[26] Yu. K. Voron'ko, A. A. Sobol', S. N. Ushakov, and L. I. Tsymbal, Neorg. Mater. **36**, 1130 (2000) [Inorg. Mater. **36**, 947 (2000)].

[27] T. T. Basiev, A. A. Sobol, P. G. Zverev, V. V. Osiko, and R. C. Powell, Appl. Opt. **38**, 594 (1999).

[28] V. Volkov, C. Cascales, A. Kling, and C. Zaldo, Chem. Mater. **17**, 291 (2005).

[29] D. Lis, E. Zharikov, K. Subbotin, Y. Voron'ko, A. Sobol, S. Ushakov, and V. Shukshin, Advanced Solid-State Photonics 2003, Feb. 2–5, 2003, San Antonio, TX, Conference edition, OSA, Paper TuB9, pp. 183–185.

[30] Yu. K. Voron'ko, E. V. Zharikov, D. A. Lis, A. A. Sobol, K. A. Subbotin, S. N. Ushakov, and V. E. Shukshin, Proc. SPIE **5478**, 60 (2004).

[31] K. A. Subbotin, E. V. Zharikov, and V. A. Smirnov, Opt. Spektrosk. **92**, 657 (2002) [Opt. Spectrosc. **92**, 601 (2002)].

[32] Yu. K. Voron'ko, E. V. Zharikov, D. A. Lis, A. A. Sobol', K. A. Subbotin, S. N. Ushakov, V. E. Shukshin, and S. Dröge, Neorg. Mater. **39**, 1509 (2003) [Inorg. Mater. **39**, 1308 (2003)].

[33] A. Ellens, H. Andres, M. L. H. ter Heerdt, R. T. Wegh, A. Meijerink, and G. Blasse, Phys. Rev. B **55**, 180 (1997).

[34] P. Porcher, M. Couto dos Santos, and O. Malta, Phys. Chem. Chem. Phys. **1**, 397 (1999).

[35] M. Rico, Ph.D. Thesis, Universidad Autónoma de Madrid, 2003.

[36] A. Méndez-Blas, M. Rico, V. Volkov, C. Cascales, C. Zaldo, C. Coya, A. Kling, and L. C. Alves, J. Phys.: Condens. Matter **16**, 2139 (2004).

[37] P.-H. Haumesser, R. Gaume, B. Viana, E. Antic-Fidancev, and D. Vivien, J. Phys.: Condens. Matter **13**, 5427 (2001).

[38] M. C. Pujol, M. A. Bursukova, F. Güell, X. Mateos, R. Solé, Jna. Gavaldà, M. Aguiló, J. Massons, F. Díaz, P. Klopp, U. Griebner, and V. Petrov, Phys. Rev. B **65**, 165121 (2002).

[39] P. Klopp, V. Petrov, U. Griebner, and G. Erbert, Opt. Express **10**, 108 (2002).

[40] S. Rivier, M. Rico, U. Griebner, V. Petrov, M. D. Serrano, F. Esteban-Betegón, C. Cascales, C. Zaldo, M. Zorn, and M. Weyers, Conference on Lasers and Electro-Optics, CLEO/Europe-EQEC'05, Munich, Germany, June 12–17, 2005, paper CF4-4-THU, Conference Digest CD-ROM.